Structure of Prismatic Halloysite

TOSHIHIRO KOGURE,[1*] KIYOFUMI MORI,[2] VICTOR A DRITS,[3] AND YOSHIZO TAKAI[2]

[1]Department of Earth and Planetary Science, Graduate School of Science, The University of Tokyo, 7-3-1 Hongo, Bunkyo-ku, Tokyo, 113-0033, Japan
[2] Department of Material and Life Science, Graduate School of Engineering, Osaka University, 2-1 Yamada-Oka, Suita, Osaka, 565-0871, Japan
[3]Geological Institute of the Russian Academy of Sciences, Pyzhevsky per 7, Moscow, Russia
*E-mail: kogure@eps.s.u-tokyo.ac.jp

Running title proposed: Structure of prismatic halloysite
Corresponding author:
Toshihiro Kogure
Department of Earth and Planetary Science, Graduate School of Science,
The University of Tokyo
7-3-1 Hongo, Bunkyo-ku, Tokyo 113-0033, Japan
E-mail: kogure@eps.s.u-tokyo.ac.jp

Revision 1
December 2012

ABSTRACT

Halloysite from Olkhon Island, Lake Baikal, Russia has been investigated using X-ray diffraction (XRD), scanning electron microscopy (SEM), selected-area electron diffraction (SAED) and, in particular, high-resolution transmission electron microscopy (HRTEM), to reveal its atomic structure and formation process. XRD analysis indicated a basal spacing of ca. 7.2 Å and two characteristic peaks with d = 4.28 and 4.03 Å on the tail of the 02, 11 band. The halloysite grain cross-sections displayed various prismatic forms, ranging from a rectangle to a regular eighteen-sectored polygon in SEM and TEM. The SAED pattern from a sector of the polygonal prisms with the incident beam parallel to the prism axes showed a regular one-layer oblique reciprocal lattice, similar to that of kaolinite along Y_i-directions. HRTEM imaging performed with the new computer-assisted minimal-dose system and an incident beam perpendicular to the prism axis showed stacking of most dioctahedral 1:1 layers with their pseudo-mirror plane perpendicular to the prism axis and an almost random, or rather, alternating lateral stagger to the right or left from the preceding layer, which corresponds to interlayer displacements of τ_+ and τ_- in Zvyagin symbols, or layer displacements of $\boldsymbol{t}_1$ and $\boldsymbol{t}_2$ used to describe the stacking in kaolinite. This stacking feature explains the SAED pattern from the side of the prismatic grains and the two characteristic peaks on the tail of the 02, 11 band in the XRD pattern. Based on these results, it is proposed that tubular halloysite initially forms as a hydrated one with the pseudo-mirror plane of the kaolinite layers perpendicular to the tube axis, then dehydrates with, possibly, partially hydrogen-bonded interlayers, and finally transforms to a prismatic one consisting of sectored flat layers with the complete hydrogen-bonded interlayers. During this transformation, stacking with comparable ratio and frequent alternation of τ_+ and τ_- is formed, to minimize morphological change of the tubes.

Keywords: halloysite, stacking sequence, prismatic form, hydrogen bonding, HRETM, SAED

INTRODUCTION

Halloysite, $Al_2Si_2O_5(OH)_4 \cdot nH_2O$, is one of the most common and ubiquitous clay minerals on the terrestrial surface. However, it is also true that the real structure of halloysite has yet to be fully understood despite the amount of research devoted to this mineral. Actually, no three-dimensional periodicity has been reported for halloysite because of very limited information from conventional diffractometry, which leads to the possibility that halloysite contains intense structural disorder. Moreover, from the standpoint of electron microscopy, halloysite is too beam-sensitive to apply recent high-resolution structure imaging in order to analyze its atomic structure.

Halloysite is one of the kaolin group minerals consisting of dioctahedral 1:1 layers which are termed "kaolinite layers" in this study, and hydrated/dehydrated interlayers. In cases involving halloysite with a tubular morphology, the kaolinite layers are rolled to compensate for the misfit between the tetrahedral and octahedral sheets (Bates et al., 1950). Bailey (1990) suggested ditrigonal rotation in the tetrahedral sheet, which reduces the misfit in the other kaolin group minerals may not be realized in halloysite due to water molecules and exchangeable cations possibly existing at the interlayer region. On the contrary, Singh (1996) proposed that the rolling mechanism of the kaolinite layers is preferable to ditrigonal rotation, if Si-Si repulsion in the tetrahedral sheet is considered. With respect to the stacking structure of halloysite, much research has suggested a two-layer periodicity for the dehydrated form, halloysite (7 Å), based on selected-area electron diffraction (SAED) taken with the incident beam perpendicular to the tube-axis (Honjo and Mihara, 1954; Honjo et al., 1954; Chukhrov and Zvyagin, 1966; Kohyama et al., 1978; Singh and Gilkes, 1992). Among them, probably only Honjo et al. (1954) and Chukhrov and Zvyagin (1966) considered the stacking structure to form the two-layer periodicity. Based on the intensity distribution in the SAED pattern, Honjo et al. (1954)

proposed a stacking sequence expressed as $\sigma_1\tau_+\sigma_1\tau_0\sigma_1$ or $\sigma_5\tau_-\sigma_5\tau_0\sigma_5$ with a triclinic symmetry, using the Zvyagin symbols (Chukhrov and Zvyagin, 1966). However, Chukhrov and Zvyagin (1966) suggested that the sequence expressed as $\sigma_3\tau_+\sigma_3\tau_-\sigma_3$ with monoclinic *Cc* symmetry could also reproduce the intensity distribution in the SAED pattern and insisted that this sequence was more realistic than that proposed by Honjo et al. (1954). In this notation, σ_3 corresponds to the intralayer displacement of $\boldsymbol{a}_o/3$ in the kaolinite layer having the orthogonal unit cell with $\boldsymbol{a}_o$ and $\boldsymbol{b}_o$ cell edges, and τ_+ and τ_- correspond to the interlayer displacements of $+\boldsymbol{b}_o/3$ and $-\boldsymbol{b}_o/3$, respectively. This sequence is also described as the regular alternation of the layer displacements (Guggenheim et al., 2009) with $\boldsymbol{a}_o/3 + \boldsymbol{b}_o/3$ ($\sigma_3\tau_+$) and $\boldsymbol{a}_o/3 - \boldsymbol{b}_o/3$ ($\sigma_3\tau_-$).

Bookin et al. (1989) showed that two-dimensional layer periodicity of defect-free 1*Tc* kaolinite can be described equally well by the orthogonal cell $\{a_o, b_o, \gamma_o\}$ ($\gamma_0 = 90^\circ$) as well as by the enantiomorphic oblique cells $\{a_1, b_1, \gamma_1\}$ and $\{a_2, b_2, \gamma_2\}$ which are related to each other by a mirror plane passing through the octahedral vacant site and the center of the ditrigonal ring of the tetrahedral sheet in kaolinite layer, and containing the $\boldsymbol{a}_o$ axis. In particular, the $\boldsymbol{a}_1$ and $\boldsymbol{a}_2$ axes of the enantiomorphic oblique cells are rotated clockwise and counterclockwise by ~120° with respect to the $\boldsymbol{a}_o$ axis. The numerical values for the oblique cells coincide with those determined for kaolinite sample from Keokuk which is almost defect-free in the stacking sequence (Suitch and Young, 1983; Bish and von Dreele, 1989), indicating that the obliquity ($\gamma_{1, 2} \neq 90^\circ$) of the refined cell of kaolinite is just the choice of the unit cell and interlayer stacking sequence does not disturb the layer symmetry. On the other hand, the layer displacements $\boldsymbol{t}_1$ and $\boldsymbol{t}_2$ which are corresponding to the individual enantiomorphs and related to each other by the mirror plane mentioned above form a defect-free 1*Tc* kaolinite structure (Bookin et al., 1989). In terms of the conventional cell (a_1, b_1, γ_1) chosen for description of a defect-free kaolinite structure, the components of the $\boldsymbol{t}_1$ and $\boldsymbol{t}_2$ are ($-0.369\boldsymbol{a}_1$, $-0.024\boldsymbol{b}_1$) and ($-0.352\boldsymbol{a}_1$, $0.304\boldsymbol{b}_1$), respectively. Bookin et al. (1989) also proposed that the stacking sequence in halloysite is

expressed as the regular interstratification of $\boldsymbol{t}_1$ and $\boldsymbol{t}_2$. The components of the $\boldsymbol{t}_1$ and $\boldsymbol{t}_2$ expressed with the orthogonal cell are $0.282\boldsymbol{a}_o + 0.327\boldsymbol{b}_o$ and $0.282\boldsymbol{a}_o - 0.327\boldsymbol{b}_o$, respectively. These expressions indicate the similarity and difference between the model by Chukhrov and Zvyagin (1966) and Bookin et al. (1989). The first authors used the layer structure with the idealized intralayer and interlayer displacements whereas the other assumed that the interlayer displacements in halloysite are identical to those in a periodic 1*Tc* kaolinite despite the quite different mutual arrangement of the adjacent layers in these structures.

Recently, Kogure et al. (2011) succeeded in recording clear two-dimensional high-resolution transmission electron microscopy (HRTEM) images from tubular halloysite, using a new TEM with a computer-assisted minimal-dose system (Hayashida et al. 2007). These images showed no symptom of a two-layer periodicity which was suggested in the previous works. They did, however, show a more likely one-layer periodicity with high density of stacking disorder. The discrepancy between two-layer periodicity and one-layer periodicity with a high density of stacking disorder should be looked into during future halloysite research.

One of the characteristic features of halloysite is its various morphologies, typical of which are tubes and spheres (see the summarized table in Joussein et al. 2005). Furthermore, Bailey (1990) described the "prismatic" form as a category of halloysite morphologies. Chukhrov and Zvyagin (1966) and Dixon and McKee (1974) showed TEM replica images in which the elongate halloysite particles had regular and flat faces parallel to the elongation of the particles. It is noteworthy that the stacking sequence reported by Chukhrov and Zvyagin (1966) as mentioned above was derived from a specimen with prismatic morphology. Beside the TEM replica images, cross sectional TEM (Bates and Comer, 1958; Singh and Gilkes, 1992, Churchman et al., 1995) and scanning electron microscopy (SEM) (Diamond and Bloor, 1970) indicated prismatic shapes for halloysite. Such prismatic morphology was proposed to be

formed during dehydration (Kirkman, 1981) or transformation from kaolinite to halloysite (Robertson and Eggleton, 1991).

Following our previous work in investigating the atomic structure of tubular halloysite using advanced electron microscopy (Kogure et al., 2011), we have investigated a different halloysite specimen which apparently shows "higher crystallinity" in X-ray diffraction (XRD). SEM observation indicated that the morphology of most grains is prismatic, similar to those reported by Chukhrov and Zvyagin (1966) and Dixon and McKee (1974). HRTEM images were successfully obtained and showed a different stacking structure from that in tubular halloysite reported in Kogure et al. (2011). Finally, experimental XRD and SAED patterns were successfully reproduced in simulation using the recorded stacking structure in these HRTEM images. These results provide new insights into the real structure of halloysite and its formation process.

SAMPLE AND METHODS

The halloysite specimen investigated was from Olkhon Island, Lake Baikal, Russia, and formed by weathering of oligoclase (Chekin et al., 1972). It was reported that the halloysite crystallites initially grew epitaxially on the (001) surface of oligoclase with a platy and dendritic shape elongated along the [100], [110], [010] and [310] directions. When the crystallites became rather thick, they peeled away from the oligoclase surface and grew as a tubular crystal along the *b*-axis with a spiral-cylindrical structure (Chekin et al., 1972, 1976).

The powder XRD pattern was measured at an ambient condition using a Rigaku RINT-Ultima^{+} diffractometer with monochromatized CuKα radiation, a 0.3 mm receiving slit, and 0.5° divergence and anti-scatter slits. A continuous scan rate of 0.1° (2θ) min^{-1} and a sampling interval of 0.02° were adopted. High-resolution SEM was conducted using a Hitachi S-4500 SEM with a cold type field-emission gun operated at 2 kV. The specimen was coated with Pt-Pd of 5 nm in thickness using a sputter coater to provide electron conductivity.

TEM specimens for cross-sectional views of the prismatic halloysite were prepared using ion-milling. The halloysite grains were mixed with epoxy resin. After hardening, the mixture was cut into slices and mechanically thinned to less than 100 μm, then made electron-transparent using an ion-milling instrument (Gatan Dual Ion Mill Model 600) with argon beams of ~ 4 KeV and an incident angle of 15°. Images and electron diffraction patterns with the prism-axis perpendicular to the beam were acquired using halloysite particles, and dispersed on holey carbon microgrids through aqueous suspension. TEM images with low magnifications and SAED patterns were acquired using JEOL JEM-2010UHR with a LaB_6 filament operated at 200 kV. The images were recorded with films or a Gatan MSC 794 bottom-mounted CCD camera, while SAED patterns were recorded with a Gatan ES-500W side-mounted CCD camera on the phosphor screen.

HRTEM images for analyzing the atomic structure in halloysite were acquired using a Hitachi HF-1000BC, with a cold field emission gun operated at 100 kV and a newly developed minimal dose system (MDS) for reducing the electron dose. The MDS consists of a CCD camera, an electric-field-type electron beam blanker that is installed beneath the condenser lens, and a computer for controlling the entire TEM system, including a CCD camera and a high speed blanker. The details for practical operation were described in our previous paper (Kogure et al., 2011). Noise contrast in the HRTEM images was removed using a Wiener-filter (Marks 1996; Kilaas 1998) developed by K. Ishizuka (HREM Research Inc.) and implemented with a Gatan DigitalMicrograph, version 3.1 0.0 (Kogure et al., 2008).

Finally, simulations of powder XRD and SAED patterns were performed using DIFFaX (Treacy et al., 1991), which calculates diffraction patterns from layered materials with stacking disorder.

RESULTS AND DISCUSSION

Powder XRD

The XRD pattern (Fig. 1a) of the specimen indicates a basal spacing of ca. 7.2 Å, suggesting that the halloysite is almost dehydrated, or halloysite-(7 Å). Apart from the basal reflections, several peaks are distinctly identified in the patterns, deviating from the XRD patterns of halloysite in other research (e.g, Joussein et al., 2005; Kogure et al., 2011). These peaks are compared with those calculated from the crystallographic parameters for kaolinite (Neder et al., 1999) in Figure 1. In the calculated patterns, the pattern for reflections with $k = 3n$ is drawn with a solid line, while that for all reflections is drawn with a broken line. First, the experimental pattern profile higher than 2θ of 35° corresponds, approximately, to the calculated pattern for kaolinite. In particular, calculated reflections with $k = 3n$ also almost make an appearance in the experimental pattern. The reflections $h \neq 0$ and $k = 3n$ are called family reflections (Ďurovič and Weiss, 1986) and their intensity distributions are distinct for the four polytypic groups (or structure types) of 1:1 phyllosilicates (Bailey, 1969; Zvyagin, 1967). The rough correspondence of the family reflections between the experimental and calculated patterns indicates that the stacking sequence in the present halloysite sample belongs to group A with a layer displacement of approximately $\pm\boldsymbol{a}_i/3$ and/or mutual rotations between adjacent layers with 0° or ±120°. On the other hand, the experimental pattern shows two characteristic peaks on the tail of the 02, 11 band, as indicated with arrows one and two. The *d*-values are 4.28 and 4.03 Å, which are in complete disagreement with the peaks for kaolinite. These *d*-values can be indexed as 021 and $\bar{1}12$ with a two-layer unit cell (Chukhrov and Zvyagin, 1966; Bailey, 1990). However, these reflections cannot be ascribed to dickite, because those for dickite have very weak intensities when compared to other reflections such as 022 or 111. On the contrary, these reflections have the strongest intensities in the 02*l*, 11*l*, and $\bar{1}1l$ reciprocal lattice rows for the stacking model proposed by Chukhrov and Zvyagin (1966). Another intense reflection, 112 with $d \sim 3.49$ Å, as expected from their model, is overlapped with 004 peaks in the powder

XRD pattern. Hence, the experimental XRD pattern in Figure 1 seems consistent with the Chukhrov and Zvyagin model.

Morphology analyses by SEM and TEM

Several secondary electron images taken by the FE-SEM are shown in Figure 2. Most halloysite grains are elongated and appear roughly cylindrical, however their cross-section is often not circular but polygonal, as indicated by the white arrows. These morphologies are very close to those reported by Chukhrov and Zvyagin (1966) and Dixon and McKee (1974), although their images are TEM replicas. In Figure 2a, the arrowed grain has a rectangular prismatic form. Such a prismatic morphology, with a small number of faces and acute angles between the adjacent faces, is commonly observed. Cross sectional TEM images of the elongated grains thinned by ion-milling are presented in Figure 3. Some grains show smoothly curved layers and appear cylindrical rather than prismatic (Fig. 3a). On the contrary, Figure 3b shows the cross section of a prismatic halloysite with five major sectors. At the boundaries of the sectors with an acute corner angle, a section of the layers are connected with a small curvature radius. It is not certain whether the void-like regions between the connected layers at the boundaries are the original structure or formed by radiation damage before the recording was completed. In Figure 3c, the cross-section is almost circular, however, a close examination of the 7 Å lattice fringes reveals that the halloysite grain also consists of many sectors. This is clearly confirmed by the SAED pattern from the grain (Fig. 3d). Eighteen intensity maximums can be counted, with an equal interval on the rings corresponding to 7.2 and 3.6 Å. Hence, the grain consists of eighteen sectors with a center angle of 20°. This structure is very similar to that of a polygonal serpentine as reported in other research, in which fifteen and thirty sectors are common (e.g., Cressey and Zussman, 1976; Yada and Wei, 1987). If we return to the SEM images in Figure 2 and examine the contrast on the surface of relatively large halloysite grains

with cylindrical forms, it can be seen that the surface consists of facets elongated parallel to the cylinder axis, as indicated with the thin black arrows in Figure 2c.

Stacking analyses using SAED and HRTEM

Figure 4 shows the cross-section of a prismatic halloysite consisting of three sectors. One half of the prism disappeared during sample preparation by ion-milling. Moreover, the areas around the center and outside of the prism were amorphized by beam radiation. The corresponding SAED pattern from the entire prism is comprised of three superimposed reciprocal lattice nets, each of which corresponds to the individual sector. The three reciprocal lattice nets are identical; one-layer periodicity, the oblique angle, and no streak, indicating the typical pattern for 1:1 phyllosilicates of group A (Bailey, 1988), which corresponds to the XRD analysis result in Figure 1. On the contrary, two-dimensional HRTEM images recorded using the TEM with a minimal dose system are shown in Figure 5. As shown in our previous paper (Kogure et al., 2011), the contrast for each kaolinite layer consists of two-tiered dark dots separated by $b/2$ (~ 4.5 Å) along the layer. Each dark dot can correspond to a pair of SiO_4 tetrahedra (or an SiO_4 chain running parallel to the incident beam) in the tetrahedral sheet and a pair of $AlO_2(OH)_4$ octahedra in the dioctahedral sheet (see Fig. 1 in Kogure and Inoue, 2005). In Figure 5, the contrast of each layer shows vertically aligned dots with no lateral shift within the layer forming a bar-like shape (indicated with a square for each layer), except for three layers in Figure 5b, which are indicated with triangles. Such contrast should appear in the HRTEM images of kaolinite viewed along [110] or [$\overline{1}\overline{1}0$] (see Fig. 3 in Kogure and Inoue, 2005). More universally, these directions are expressed as those parallel to the pseudo-mirror plane described by Bookin et al. (1989), passing through both the octahedral vacant site and center of the tetrahedral six-membered ring in the kaolinite layer. Moreover, such contrast for each kaolinite layer is laterally shifted to the right or left against that for the lower and upper layers in the amount of

249 *b*/6 (only two exceptions are indicated with the white arrows in Figure 5c, where no lateral shift
250 is observed). As described in Kogure and Inoue (2005), these right and left shifts correspond to
251 the projections of the layer displacements for $\boldsymbol{t}_1$ and $\boldsymbol{t}_2$ (In actuality, they are related to each
252 other through the pseudo-mirror plane), or directly correspond to the Zvyagin's interlayer shifts
253 of τ_+ and τ_-. Hence, the two-layer stacking model proposed by Chukhrov and Zvyagin (1966)
254 should appear as the alternating shift of the contrast for the kaolinite layer in Figure 5. However,
255 such alternation is only observed locally (indicated with square brackets in the figure) with six
256 or seven layers, and not in the entire stacking.
257 As mentioned above, two-layer periodicity was proposed for the stacking structure of
258 halloysite, based on electron diffraction from tubular grains in previous researches pertaining to
259 halloysite (Honjo and Mihara, 1954; Honjo et al., 1954; Chukhrov and Zvyagin, 1966,
260 Kohyama et al., 1978; Singh and Gilkes, 1992). Previous research found the intensity
261 maximum at a position parallel to the tube axis on the 02*l* row, which can be indexed 020. On
262 the 02*l* row, the next intensity peak to 020 has a distance that nearly corresponds to two-layer
263 periodicity, which is perhaps the reason why the two-layer structure was proposed. However,
264 the 02*l* diffraction rows in their SAED patterns are considerably streaked, except for that
265 presented by Chukhrov and Zvyagin (1966). It is possible that these patterns were obtained with
266 a selected-area aperture including the whole diameter of the tubular form. In this case, the
267 intensity maximum will be formed at the 020 position by the streaked 02*l* diffraction row from
268 the top and/or bottom parts of the tubular wall normal to the electron beam. Figures 6b and c
269 show examples of the SAED patterns from the present specimen, obtained by including the
270 whole diameter (Fig. 6b) and only the side region of the prism (Fig. 6c), using the selected-area
271 apertures drawn in Figure 6a. The intensity maximum at the 020 position as indicated with the
272 white arrows in Figure 6b does not appear in Figure 6c. Most halloysite prisms which are thick
273 enough to set the aperture as in Figure 6a showed similar results; they did not indicate two-layer

periodicity. However, occasionally the intensity maximum appeared at the 020 position in the SAED pattern from the side region of a prism, implying that the possibility of a two-layer structure could not be fully excluded.

Simulation of XRD and SAED pattern

Another issue to be considered is the origin of the two characteristic peaks at the 02, 11 band with d = 4.28 and 4.03 Å in the XRD pattern (Fig. 1), which were indexed as 021 and $\bar{1}12$ with a two-layer structure. In Figure 5, the HRTEM images indicate almost the same intralayer displacement (σ_3 of the Zvyagin symbol) and heavily disordered interlayer displacement with τ_+ and τ_- (or layer displacement with $\boldsymbol{t}_1$ and $\boldsymbol{t}_2$). Powder XRD and SAED patterns from this structure model have been simulated using DIFFaX (Treacy et al., 1991). Such a simulation for XRD was already performed by Bookin et al. (1989), but their result (Fig. 6 in their paper) is confusing owing to an editorial mistake. The same result presented in Drits and Tchoubar (1990) is preferable as a reference.

The calculation procedure is similar to our previous research (Kogure et al., 2006a; Kogure et al., 2010). The lattice constants and atomic coordinates for the kaolinite layer were derived from the results by Neder et al. (1999) and coordinates for $\boldsymbol{t}_1$ and $\boldsymbol{t}_2$ are those described in Bookin et al. (1989) as described above. To make the calculation more simple, we assume equal proportions for $\boldsymbol{t}_1$ and $\boldsymbol{t}_2$ ($W_1 = W_2 = 0.5$). Accordingly, all of the condition probabilities (P_{11}, P_{12}, P_{21}, P_{22}) are determined if one of them, e.g., P_{11}, is specified (Bookin et al., 1989), where P_{11} refers to the probability that $\boldsymbol{t}_1$ comes next to $\boldsymbol{t}_1$ in the stacking. Figure 7 shows the calculated XRD patterns with various P_{11} values, and the experimental one for comparison. We adopted a pseudo-Voigt function with the same ratio of Gaussian and Lorentz shapes and a half-width of 0.1° for the peak profile. In Figure 7, P_{11} = 0 corresponds to the stacking model by Chukhrov and Zvyagin (1966) and Bookin et al. (1989) with two-layer periodicity, and P_{11} =1 to the

segregated two enantiomeric kaolinite crystals with one-layer periodicity. Based on the figure, it is understood that the two characteristic peaks at the 02, 11 band in the experimental pattern are reproduced in the wide range of P_{11}, from $P_{11} = 0$ to even the most disordered state of $P_{11} = 0.5$. The peaks corresponding to those for kaolinite appear from $P_{11} = 0.7$. Hence, the two peaks in the experimental pattern do not necessarily indicate ordered two-layer periodicity, but only a tendency towards it.

The calculated intensity distributions along the reciprocal row next to 00*l* in the SAED patterns in Figure 6c were also calculated using DIFFaX and shown in Figure 8. As the disorder increases, the peaks are broadened and those with $l = 2n$ disappear, losing any evidence of two-layer periodicity. The twin maximums at $l = \pm 1$ correspond to those in the SAED pattern in Figure 6c and they also correspond to the peak with $d = 4.28$ Å in the XRD pattern. The intensity maximums corresponding to the peak with $d = 4.03$ Å in the XRD pattern are on the other reciprocal rows. As P_{11} exceeds 0.5, these peaks move and split and finally ($P_{11} = 1.0$) the pattern becomes that of the 11*l* diffraction row from the two enantiomeric kaolinite crystals.

Formation and ripening process of halloysite

When summarizing the result of the analysis described above, the crystal structure of prismatic halloysite is expressed as an almost-ordered layer orientation (intralayer displacement) and heavily-disordered layer displacement with $\boldsymbol{t}_1$ and $\boldsymbol{t}_2$. This expression is almost the same as the conclusions for disordered kaolinite by Plançon et al. (1989) derived using XRD and Kogure and Inoue (2005) using HRTEM. However, to the best of our knowledge, similar peaks on the 02, 11 band observed in the XRD pattern of the present specimen were not reported for disordered kaolinite. As the XRD simulation indicated, the origin of these peaks is of comparable proportion to $\boldsymbol{t}_1$ and $\boldsymbol{t}_2$, and their frequent alternation ($P_{11} \leq 0.5$). Hence, this is characteristic of the structure of prismatic halloysite. Although there are

not a significant number of successful HRTEM images, it is probable that the pseudo-mirror plane in the kaolinite layer being perpendicular to tube or prismatic axis, or the kaolinite layer rolling around the axis normal to the pseudo-mirror plane could represent other structural characteristics of halloysite. The origin of these features will be considered in the following paragraph (Fig. 9).

It seems natural and undisputed that initially halloysite grows as a hydrated form, halloysite (10Å), without hydrogen, bonds between the basal oxygen and hydroxyl across the interlayer. It is probable that the roll direction of the layer at this initial stage is the same as that found in the present specimen, about the normal of the pseudo-mirror plane in the kaolinite layer (Fig. 9a). Although we have no evidence, it is suspected that the dioctahedral 1:1 layer can bend more easily along this direction to relax the lateral misfit between the tetrahedral and octahedral sheets. Next, the water molecules are removed from the interlayer to form halloysite (7Å) (Fig. 9b). At this stage, because the layers are not flat but cylindrical, and cannot realize the specific positional relation between adjacent layers all over the circumference, hydrogen bonding across the interlayer must be limited in a circuit. Although the number of successful HRTEM images was limited, Kogure et al. (2011) reported the stacking structure of cylindrical halloysite with a pseudo-mirror plane normal to the tube axis and no lateral stagger between adjacent layers, as illustrated in Figure 9b. In this configuration, $\boldsymbol{t}_1$ or $\boldsymbol{t}_2$ layer displacement, which forms stable hydrogen bonding in kaolinite, does not exist. During the probable long-term ripening of halloysite cylindrical forms are converted to prismatic ones with sector domains in which the kaolinite layers are flat. During this deformation, each layer moves relative to the adjacent layer by $\pm b/3$ (or $\pm b/6$) along the tube-axis (the black arrows in Figure 9b), to form an interlayer configuration with hydrogen bonding such as that in kaolinite (Fig. 9c). At this time, in order to minimize deformation of the external form of halloysite, the proportion of the displacements of $+ b/3$ ($= \tau_+$) and $- b/3$ ($= \tau_-$) should be comparable and they should make frequent exchanges

along the stacking as can be seen via the black arrows in Figure 9b, which results in a P_{11} value less than 0.5.

CONCLUDING REMARKS

If our model for the stacking structure and its formation pathway is accurate, the structural difference between kaolinite and halloysite is related to their formation processes. For kaolinite, the crystals grow *via* layer by layer or spiral growth mechanisms (e.g., Kogure et al., 2010). During these growth processes, a new kaolinite layer and hydrogen bonding at the interlayer is formed simultaneously. Our previous HRTEM research (Kogure and Inoue, 2005; Kogure et al., 2010) reported that stacking structure regarded as "growth faults" (Bookin et al., 1989) or "enantiometric twins" (Kogure et al., 2010) which are formed with a condition probability P_{11} more than 0.5 are common in kaolinite. This implies that, in kaolinite, stacking with the same layer displacement to the adjacent layer is thermodynamically more favorable than stacking with the different layer displacement. In prismatic halloysite, by contrast, our model suggests that the hydrogen bonds in the interlayer are generated after the formation of concentric or spiraled kaolinite layers. In this case, it is probable that the kinetic factor to minimize the deformation of the external shape to form hydrogen bonding promotes the tendency to form a regular interstratification of the different layer displacements.

ACKNOWLEDGMENTS

The authors are grateful to E. Fujii for the XRD measurements and preparation of the specimens for SEM and TEM. The authors also thank to M. Mellini and G.J. Churchman for their reviews of the manuscript and valuable suggestions. This work was supported by Grants-in-Aid for Scientific Research 24340133 and 21107005 from the Japan Society for the Promotion of Science (JSPS) and Ministry of Education, Culture, Sports, Science and Technology (MEXT), respectively. V.A. Drits acknowledges the Russian Foundation for Basic Research, Grant 2012-05-00381.

REFERENCES CITED

Bailey, S.W. (1969) Polytypism of trioctahedral 1:1 layer silicates. *Clays and Clay Minerals*, **17,** 355-371.

Bailey, S.W. (1988) Polytypism of 1:1 layer silicates. In S.W. Bailey, Ed., Hydrous Phyllosilicates (Exclusive of Micas), p. 9-27. Reviews in Mineralogy, Mineralogical Society of America, Washington, D.C.

Bailey, S.W. (1990) Halloysite – A critical assessment. In: Farmer, V.C and Tardy, Y. (Eds), Proceedings of the 9th International Clay Conference, Strasbourg, France. Sci. Geol. Mem. 86: 89-98.

Bates, T.F. and Comer, J.J. (1958) Further observations on the morphology of chrysotile and halloysite. Clays and Clay Minerals, 6, 237-248.

Bates, T.F., Hildebrand, F.A., and Swineford, A. (1950) Morphology and structure of endellite and halloysite. American Mineralogist, 35, 463-484.

Bish, D.L. and von Dreele, R.B. (1989) Rietveld refinement of non-hydrogen atomic positions in kaolinite. Clays and Clay Minerals, 37, 289-296.

Bookin, A.S., Drits, V.A., Plançon, A., and Tchoubar, C. (1989) Stacking faults in kaolin-group minerals in the light of real structural features. Clays and Clay Minerals, 37, 297-307.

Chekin S.S., Samptoin N.D., and Finko, V.I. (1972) Formation of halloysite by weathering of oligoclase. Izvestiya Akademii Nauk SSSR, Seriya geologicheskaya, N11, 88-114 (in Russian).

Chekin, S.S., Samotoin, N.D., and Finko, V.I. (1976) Spiral-cylindrical shape and growth of halloysite crystallites. Izvestiya Akademii Nauk SSSR, Seriya geologicheskaya, N 6, 111-124 (in Russian).

Chukhrov, F.V. and Zvyagin, B.B. (1966) Halloysite, a crystallochemically and mineralogically distinct species. Proceedings of the International Clay Conference, 1966 (L. Heller and A. Weiss, editors). Israel Program for Scientific Translation, Jerusalem, Israel.

Churchman, G.J., Davy, T.J., Aylmore, L.A.G, Gilkes, R.J. and Self, P.G. (1995) Characteristics of fine pores in some halloysites. Clay Minerals, 30, 89-98.

Cressey, B.A. and Zussman, J. (1976) Electron microscopic studies of serpentinites. Canadian Mineralogist, 14, 307-213.

Diamond, S. and Bloor, J.W. (1970) Globular cluster microstructure of endellite (hydrated halloysite) from Bedford, Indiana. Clays and Clay Minerals, 18, 309-312.

Dixon, J.B. and McKee, T.R. (1974) Internal and external morphology of tubular and spheroidal halloysite particles. Clays and Clay Minerals, 22, 127-137.

Drits, V.A. and Tchoubar, C. (1990) X Ray Diffraction by Disordered Lamellar Structures: Theory and Applications to Microdivided Silicates and Carbons. Berlin; Tokyo: Springer-Verlag, XVII+648 pp.

Ďurovič, S. and Weiss, Z. (1986) OD structures and polytypes. Bulletin de Minéralogie, 109, 15-29.

Guggenheim, S., Adams, J.M., Bergaya, F., Brigatti, M.F., Drits, V.A., Fromoso, M.L.L., Galan, E., Kogure, T., Stanjek, H., and Stucki, J.W. (2009) Nomenclature for stacking in phyllosilicates: Report of the Association Internationale pour l'Etude des Argiles (AIPEA) nomenclature committee for 2008, Clay Minerals, 44, 157-159.

Hayashida, M., Nomaguchi, T., Kimura, Y., and Takai, Y. (2007) Development of computer-assisted minimal dose system with beam blanker for TEM. Micron, 38, 505-512.

Honjo, G. and Mihara, K. (1954) A study of clay minerals by electron-diffraction diagrams due to individual crystallites. Acta Crystallographica, 7, 511-513.

Honjo, G., Kitamura, N., and Mihara, K. (1954) A study of clay minerals by means of single-crystal diagrams – the structure of tubular kaolin. Clay Minerals Bulletin. 2, 133-141.

Joussein, E., Petit, S., Churchman, J., Theng, B., Righi, D., and Delvaux, B. (2005) Halloysite clay minerals – a review. Clay Minerals, 40, 383-426.

Kilaas, R. (1998) Optimal and near-optimal filters in high-resolution electron microscopy. Journal of Microscopy, 190, 45-51.

Kirkman, J.H. (1981) Morphology and structure of halloysite in New Zealand tephras. Clays and Clay Minerals, 29, 1-9.

Kogure, T. and Inoue, A. (2005a) Determination of defect structures in kaolin minerals by high-resolution transmission electron microscopy (HRTEM). American Mineralogist, 90, 85-89.

Kogure, T., Jige, M., Kameda, J., Yamagishi, A., Miyawaki, R., and Kitagawa, R. (2006a) Stacking structures in pyrophyllite revealed by high-resolution transmission electron microscopy (HRTEM). American Mineralogist, 91, 1293-1299.

Kogure, T., Kameda, J., Matsui T., and Miyawaki, R. (2006b) Stacking structure in disordered talc: interpretation of its X-ray diffraction pattern by using pattern simulation and high-resolution transmission electron microscopy. American Mineralogist, 91, 1363-1370.

Kogure, T., Eilers, P.H.C., and Ishizuka, K. (2008) Application of optimum HRTEM noise filters in mineralogy and related sciences. Microscopy and Analysis, 22, S11-S14.

Kogure, T., Johnston, C.T., Kogel, J.E. and Bish, D. (2010) Stacking disorder in a sedimentary kaolinite. Clays and Clay Minerals, 58, 63-72.

Kogure, T., Mori, K., Kimura, Y. and Takai, Y. (2011) Unraveling the stacking structure in tubular halloysite using a new TEM with computer-assisted minimal-dose system, American Mineralogist, 96, 1776-1780

Kohyama, N., Fukushima, K. and Fukami, A. (1978) Observation of hydrated form of tubular

446 halloysite by an electron microscope equipped with an environmental cell. Clays and Clay
447 Minerals, 26, 25-40.
448 Marks, L.D. (1996) Wiener-filter enhancement of noisy HREM images. Ultramicroscopy, 62,
449 43-52.
450 Neder, R.B., Burghammer, M., Grasl, T., Schulz, H., Bram, A., and Fiedler, S. (1999)
451 Refinement of the kaolinite structure from single-crystal synchrotron data. Clays and Clay
452 Minerals, 47, 487-494.
453 Plançon, A., Giese, R.F., Snyder, R., Drits, V.A., and Bookin, A.S. (1989) Stacking faults in the
454 kaolin-group minerals - defect structures of kaolinite. Clays and Clay Minerals, 37, 203-210.
455 Robertson, I.D.M. and Eggleton, R.A. (1991) Weathering of granitic muscovite to kaolinite and
456 halloysite and of plagioclase-derived kaolinite and halloysite. Clays and Clay Minerals, 39,
457 113-126.
458 Singh, B. (1996) Why does halloysite roll? A new model. Clays and Clay Minerals, 44,
459 191-196.
460 Singh, B. and Gilkes, R.J. (1992) An electron optical investigation of the alteration of kaolinite
461 to halloysite. Clays and Clay Minerals, 40, 212-219.
462 Suitch, O.R. and Young, R.A. (1983) Atomic position in highly ordered kaolinite. Clays and
463 Clay Minerals, 31, 357-366.
464 Treacy, M.M.J., Newsam, J.M. and Deem, M.W. (1991) A general recursion method for
465 calculating diffracted intensities from crystals containing planar faults. Proceedings of the
466 Royal Society of London A, 433, 499-520.
467 Yada, K. and Wei, L. (1987) Polygonal microstructures of Povlen chrysotile observed by
468 high-resolution electron microscopy. Abstracts Sixth Meeting of the European Clay Groups
469 (Seville), 596-597.

Zvyagin, B.B. (1967) Electron diffraction analysis of clay mineral structures. New York: Plenum Press, XVI+364 pp.

Figure captions.

FIGURE 1. XRD pattern of halloysite from Olkhon Island, Lake Baikal, Russia, taken at ambient conditions. The calculated patterns for kaolinite including all reflections and those with $k = 3n$ are also plotted for comparison. Although they are broadened, most halloysite peaks are also identified in the calculated kaolinite pattern with $k = 3n$. However, those indicated with the arrows 1 and 2 on the 02, 11 band do not correspond to kaolinite.

FIGURE 2. FE-SEM images of the halloysite, showing polygonal cross-sections as indicated with the white arrows. The thin black arrows in (c) indicate that the surface of the cylindrical halloysite actually consists of elongated faces parallel to the cylindrical axis (see also Fig. 3c).

FIGURE 3. (a-c) Cross-sectional TEM images of several prismatic halloysites. (d) SAED pattern from the cross-section in (c). The two arrows indicate the ring corresponding to 7.2 and 3.6 Å. Eighteen intensity maximums with an almost equal interval are observed in the rings, indicating that the prism is actually a regular octadecagon with eighteen sectors.

FIGURE 4. (left) Cross-section of a prismatic halloysite with three major sectors. One-half of the prism in the top-left disappeared during the ion-milling sample preparation. In addition, the crystals around the center and outer surface amorphized before TEM recording. (Right) The SAED pattern from the prism is comprised of a superposition of three reciprocal lattices. Three sectors in the image correspond to the numbered reciprocal lattices.

498

499 **FIGURE 5.** (a) Low-magnified image of a halloysite grain, showing the area of the HRTEM
500 image in (b). Filtered HRTEM image in the rectangle in (a). The squares and triangles at the
501 individual kaolinite layers indicate the types of contrast relating to the layer orientation defined
502 in Kogure and Inoue (2005). The square bracket indicates a position where the stacking is
503 regarded as the two-layer structure proposed by Chukhrov and Zvyagin (1966). (c) Filtered
504 HRTEM image of the side of another prismatic grain, showing a similar contrast. The
505 interlayers indicated with white arrows show no lateral shift between the contrasts at the two
506 layers across the interlayer.

507

508 **FIGURE 6.** (a) Bright-field TEM image of a thick halloysite prism, showing the position and
509 size of selected-area aperture used to acquire the SAED patterns in (b) and (c). (b) SAED
510 pattern from the area selected by the larger aperture with "b" in (a). (c) SAED pattern from the
511 side of the prism, using the smaller aperture with "c" in (a). Note that the intensity maximums
512 indicted with the arrows in (b), which were previously considered the 020 peak, have almost
513 disappeared in (c). The white bracket in (c) indicates the diffraction row and its range for which
514 the intensity distribution is simulated in Figure 8.

515

516 **FIGURE 7.** Simulated XRD patterns for halloysite as a function of P_{11}, the condition
517 probability to continue the layer displacement of $\boldsymbol{t}_1$ over $\boldsymbol{t}_1$. The experimental pattern is also
518 shown at the top.

519

520

521 **FIGURE 8.** Calculated intensity distribution on the diffraction rows next to 00*l* in the SAED
522 pattern in Figure 6c. The unit for the horizontal axis is the value of *l* for two-layer periodicity.
523 The experimental intensity distribution along the diffraction row indicated with the white
524 bracket in Figure 6c is also shown at the top.

525

526 **FIGURE 9.** Schematic drawing for the ripening pathway of halloysite. See the text for details.

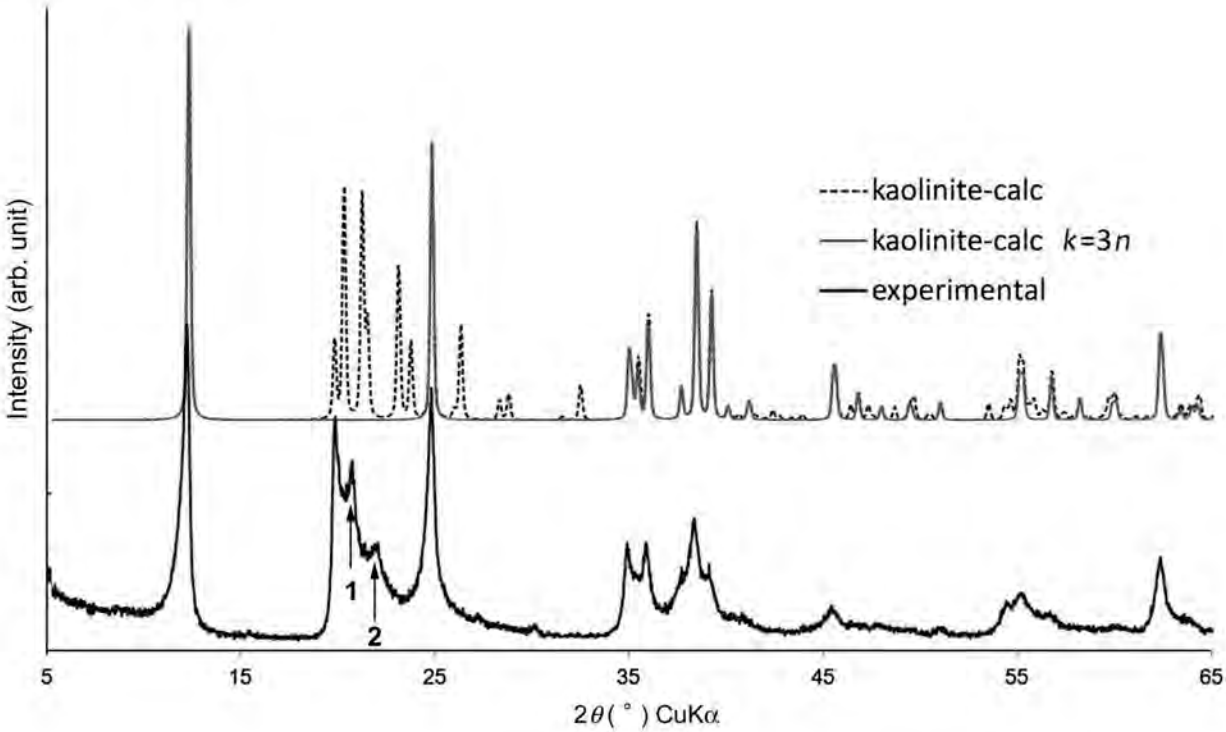

Kogure et al., Figure 1

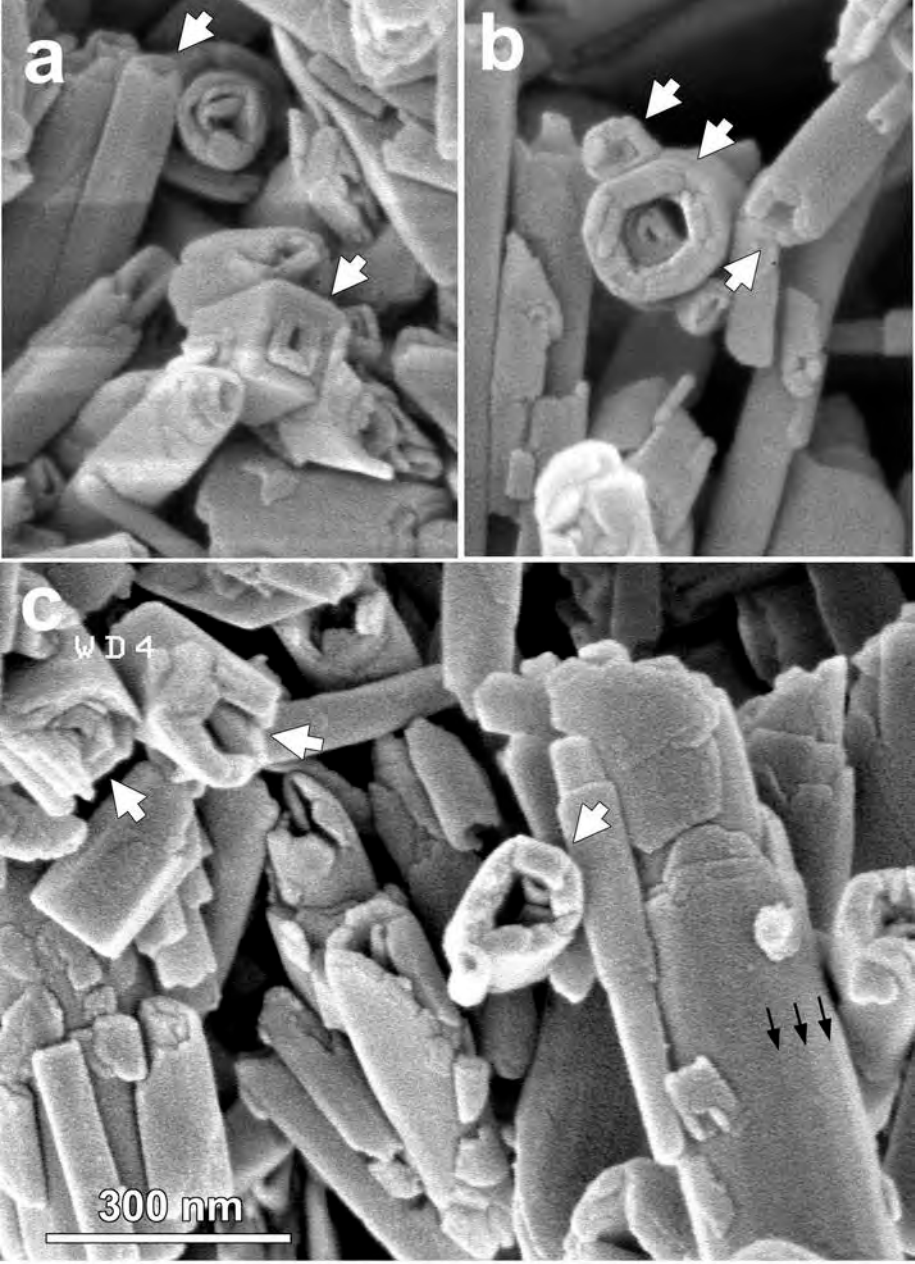

Kogure et al., Figure 2

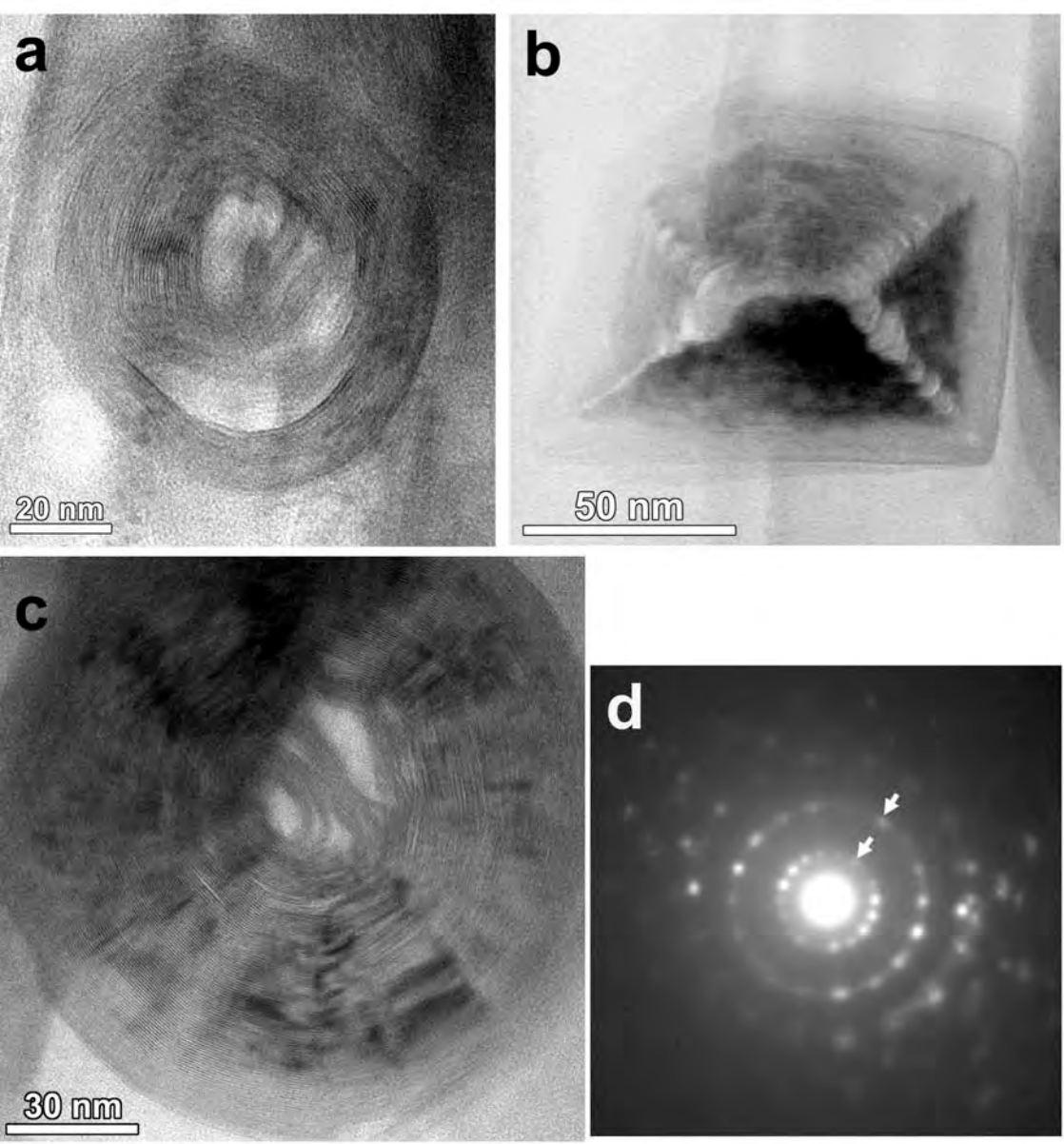

Kogure et al., Figure 3

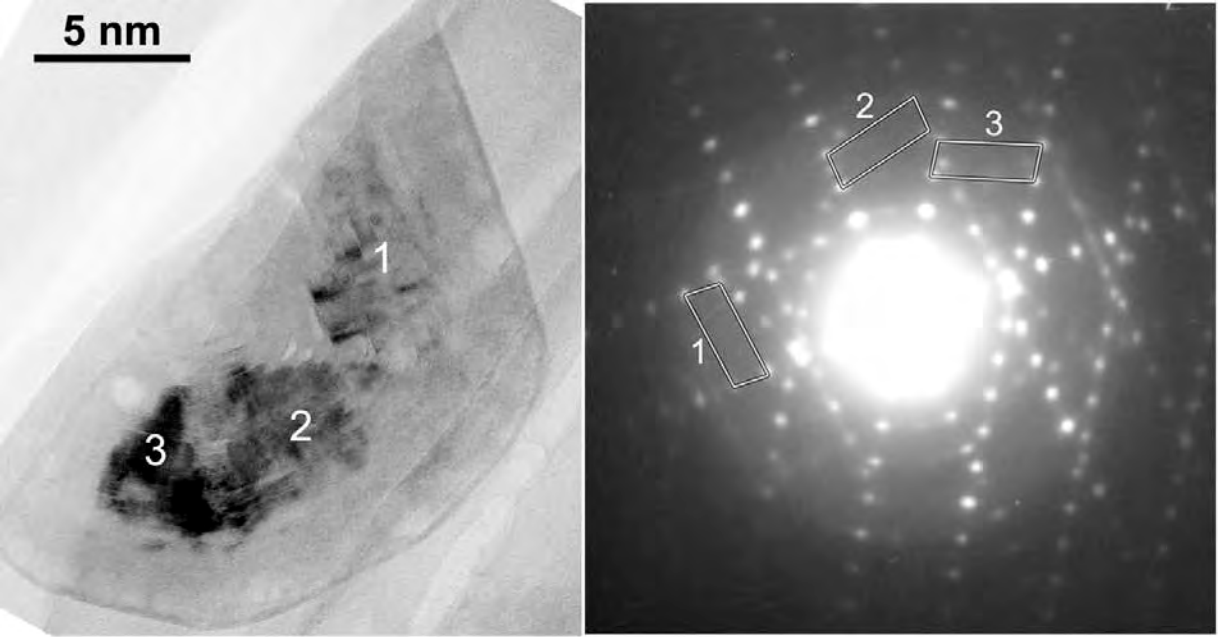

Kogure et al., Figure 4

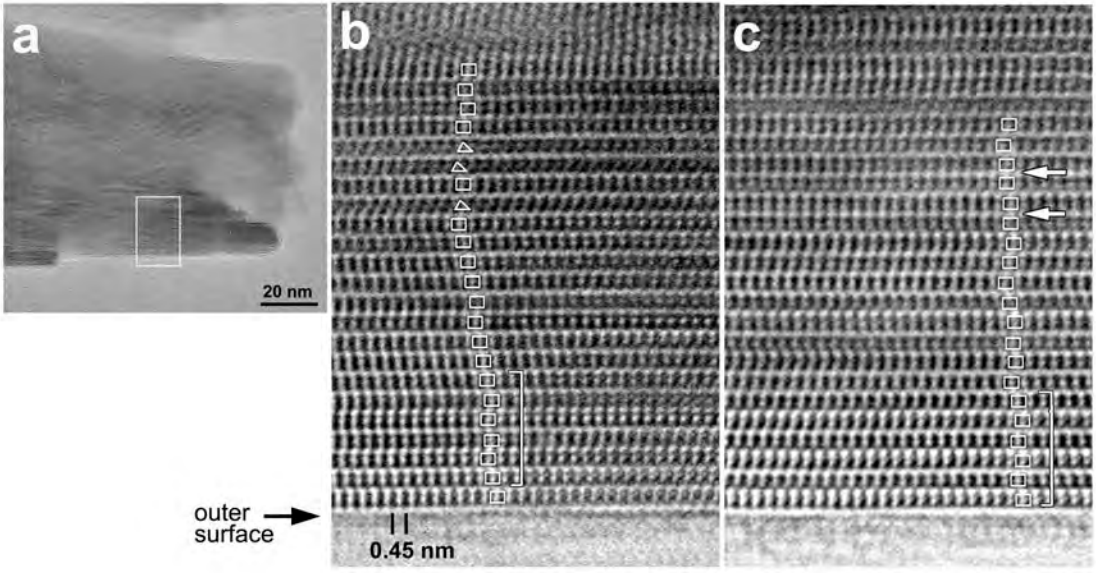

Kogure et al., Figure 5

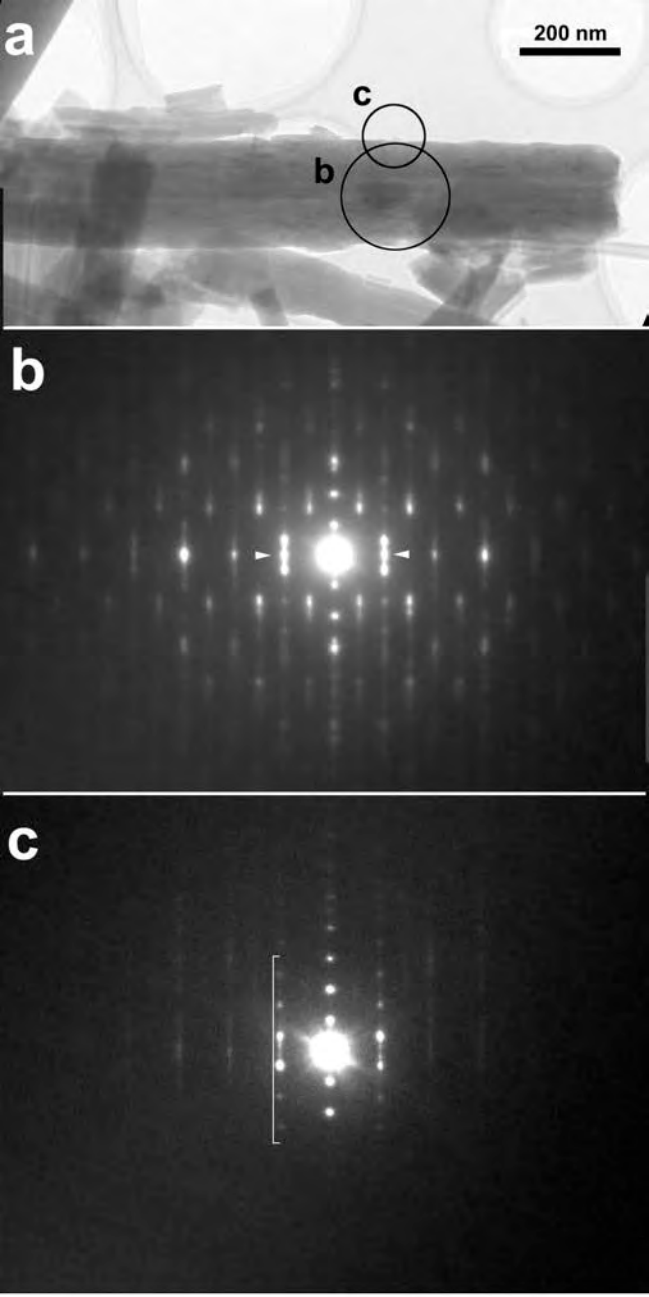

Kogure et al., Figure 6

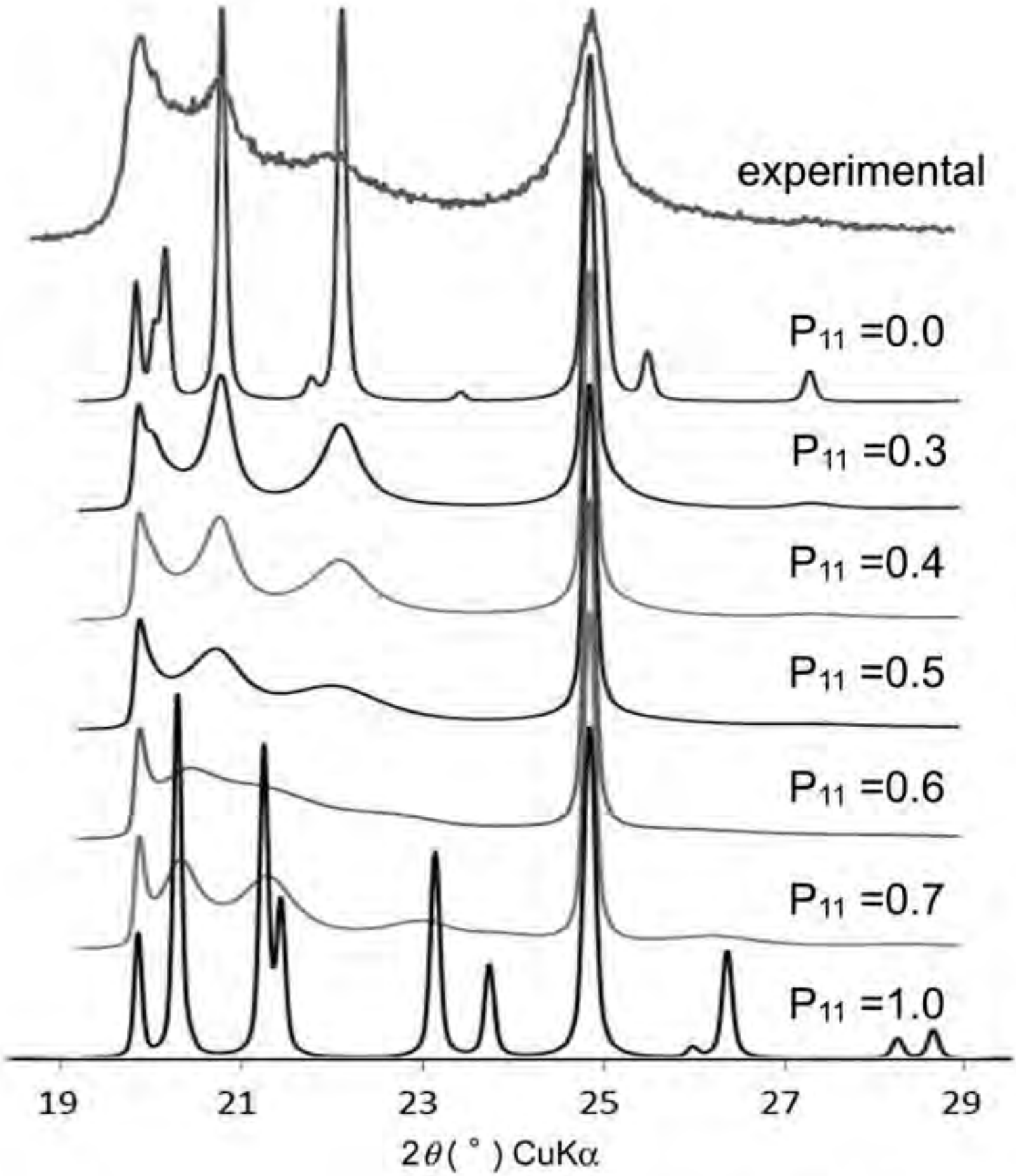

Kogure et al., Figure 7

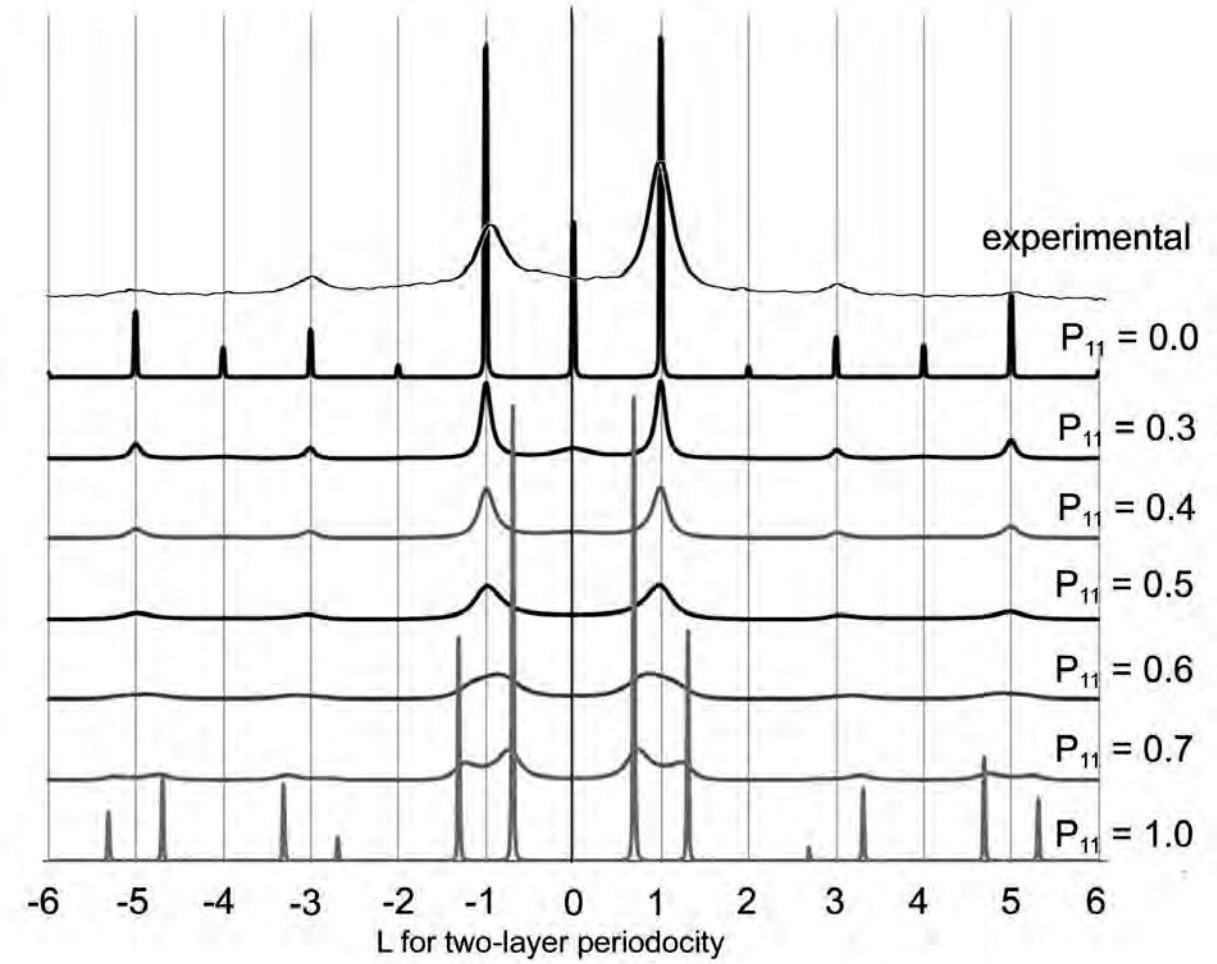

Kogure et al., Figure 8

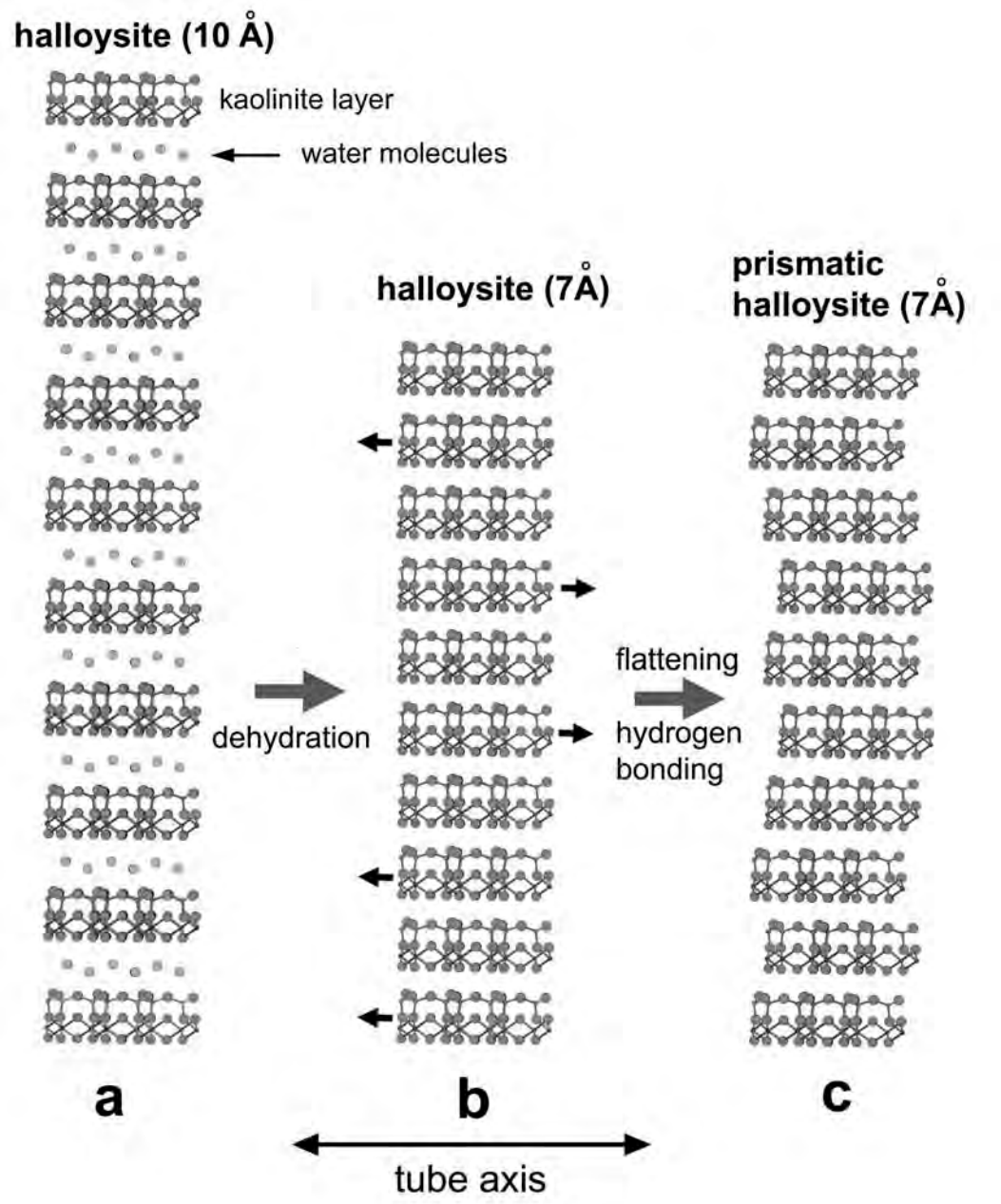

Kogure et al., Figure 9